Delayed CO_2 emissions from ocean ridges as the cause of late-Pleistocene glacial cycles

Peter Huybers and Charles H. Langmuir

Harvard University, 20 Oxford St., Cambridge MA

Abstract

The coupled 100,000 year variations in ice volume, temperature, and atmospheric CO_2 during the late Pleistocene are generally considered to arise from a combination of changes in orbital forcing, ice dynamics, and ocean circulation. It has also been argued that volcanic contributions induced by changes in glaciation influence atmospheric CO_2 and act as a feedback upon variations in glaciation. Beyond acting as a feedback, here it is suggested that ocean ridge volcanism plays an important role in generating late-Pleistocene 100 ky glacial cycles. Opposing pressure variations associated with deglaciation on land and rising sea level would merely cause offsetting volcanic CO_2 contributions except that anomalies in the flux of CO_2 from ocean ridges require tens-of-thousands of years, or longer, to ascend from the base of the melt zone and emit into the ocean. A simple model involving temperature, ice, and CO_2 is presented that oscillates at $\sim$100 ky time scales when incorporating a delayed CO_2 contribution from ridges, even if the feedback accounts for only a small fraction of total changes in CO_2. Oscillations become phase-locked with insolation forcing from changes in Earth's orbit and, under certain parameterizations, transition from $\sim$40 ky to larger $\sim$100 ky oscillations during the mid-Pleistocene Transition in response to modulations in the amplitude of obliquity. This novel description of Pleistocene glaciation should be testable through ongoing advances in understanding the circulation of carbon in the solid earth.

Keywords: Pleistocene, , glacial cycles, volcanism

1. Introduction

A satisfactory explanation of Late-Pleistocene glacial cycles also requires explanation of the accompanying changes in atmospheric CO_2 (Broecker, 2013). This view is supported by several lines of evidence. A nearly in-phase relationship of changes in Antarctic temperature and CO_2 during deglaciations suggest the importance of CO_2 for driving changes in glaciation (Pedro et al., 2012; Parrenin et al., 2013). A leading role for CO_2 is also supported by observations of globally coordinated maxima in ice extent between 25-18 ka during low CO_2 conditions and their subsequent retreat following rising CO_2 between 18-11 Ka (e.g. Shakun et al., 2012; Putnam et al., 2013; Kelly et al., 2014). The fact that glacier retreat is coordinated between the mid-latitudes of the Northern and Southern Hemispheres appears particularly telling because insolation anomalies associated with precession are opposite between the hemispheres (Doughty et al., 2015). Circulation changes can also globalize local anomalies, but atmospheric model simulations suggest that Northern Hemisphere climate change would not drive a coordinated retreat in Southern Hemisphere glaciation through changes in either temperature or precipitation (Manabe and Broccoli, 1985; Lee et al., 2011).

Despite its central role, why CO_2 changes between glacials and interglacials remains poorly understood. Warming leads to decreased ocean CO_2 solubility, but this effect is probably more than counteracted by uptake of carbon associated with regrowth of the biosphere Crowley (1995); Peterson et al. (2014), leaving the approximately 80 ppm rise in atmospheric CO_2 during late-Pleistocene deglaciations to more speculative mechanisms. Most hypotheses focus on the role of the Southern Ocean in releasing CO_2 back to the atmosphere. This flux could variously be influenced by changes in stratification (Gildor et al., 2002), the location of the westerly winds (Toggweiler et al., 2006), Antarctic sea ice extent (Ferrari et al., 2014), or iron fertilization (Jaccard et al., 2013). There is evidence for increased nutrient utilization in the Southern Ocean during the last ice age (Martínez-García et al., 2014) and for increased fluxes of respired CO_2 to the surface of the Southern Ocean during the last deglaciation (Anderson et al., 2009; Sigman et al., 2010), consistent with Southern Ocean control of glacial-interglacial atmospheric CO_2 variability.

2

It is not clear, however, whether the glacial ocean released sufficient carbon to fully explain glacial-interglacial changes in atmospheric CO_2. Gradients in surface to mid-depth radiocarbon activity are not appreciably greater in the Pacific during the glacial (Broecker et al., 2008; Lund, 2013); deep Pacific carbonate ion concentrations do not appreciably change over the last glacial cycle (Yu et al., 2013); and there is appears no widespread excess in preservation of carbonates during deglaciation (Mekik et al., 2012). This degree of stability in indicators of the marine carbon cycle does not rule out glacial oceans storing sufficient carbon to explain atmospheric CO_2 variations because proxy interpretation is uncertain and spatial coverage limited, but it does admit for the possibility of complimentary non-oceanic carbon sources (Broecker et al., 2015).

Variations in volcanic CO_2 emissions have also been suggested to contribute to glacial-interglacial CO_2 variations. Arrhenius and Holden (1897) credit Hogbom for arguing that glacial-interglacial variations could be caused by anomalous volcanic CO_2 emissions—as well as for motivating efforts to calculate the radiative forcing associated with changes in atmospheric CO_2 concentration (Arrhenius, 1896). More recent evidence for volcanic responses to variations in glaciation and sea level motivates further consideration of whether and how volcanism could, in turn, influence glacial variability.

Regional studies indicate that subaerial volcanism increased with deglaciation (e.g. Jellinek et al., 2004; Bacon and Lanphere, 2006; Nowell et al., 2006; Licciardi et al., 2007; Rawson et al., 2016). Such an increase can be understood as a consequence of deglaciation depressurizing volcanoes, and the lower pressure leading to a greater probability of eruption because of increased magmatic melt (Maclennan et al., 2002) and reduced confining pressure (Jellinek et al., 2004). Far field affects associated with lithospheric flexure may also be relevant. Huybers and Langmuir (2009, hereafter HL09) analysed two compilations of subaerial volcanic events (Bryson et al., 2006; Siebert et al., 2010) and estimated an increase in global eruption frequency during the last deglaciation, peaking at 2-6 times above modern levels during the latter half of the deglaciation. A more recent study using similar datasets (Watt et al., 2012) and another using a compilation of large eruptions (Brown et al., 2014) also support a global increase in volcanism, albeit with increases at the lower end of HL09's range. Anal-

ysis of ash layers recorded in marine sediment records also indicates that subaerial volcanism responded to changes in glaciation (Kutterolf et al., 2013).

Sustained, major changes in subaerial volcanism have consequences for atmospheric CO_2 concentrations. Assuming that changes in CO_2 emissions are proportional to global eruption rates, HL09 estimated that increased subaerial volcanism contributes between 15-70 ppm of the rise in atmospheric CO_2 concentrations during the second half of the deglaciation. Such volcanic emissions may help explain the noted stability of certain carbon cycle indicators between glacial and interglacial conditions through reducing the total amount of carbon that otherwise must be extracted from the glacial ocean (Broecker et al., 2015). Roth and Joos (2012) examined HL09's emission scenarios in a more complete carbon model, including sediment contributions to the carbon cycle. They first discuss that only the lower range of HL09's emission scenario is consistent with the shape of the CO_2 curve and lack of widespread marine carbonate dissolution during the last deglaciation, but Roth and Joos (2012) then obtain good agreement between observations and model results using HL09's central emission scenario after also accounting for the effects of regrowth of the terrestrial biosphere.

Deglaciation has the obvious downstream effect of raising sea level, which has consequence for marine volcanism. Melt is produced at marine ridges by depressurization of the mantle during ascent. Deglacial rises in sea level on the order of 1 cm per year suppress about 10% of melt generation, given an average mantle ascent of three cm per year and seawater being roughly a third the density of the mantle. HL09 suggested that such anomalies in melt production would lead to identifiable signals in ridge bathymetry. Crowley et al. (2015) showed how the magnitude of the melt response depends upon both ridge spreading rates and the period of sea level variability, and they presented evidence from the Australian-Antarctic ridge supporting a bathymetry response to Pleistocene variations in sea level. East Pacific Rise bathymetry may also show a response to sea level (Tolstoy, 2015), though whether surface bathymetry signals should be identifiable at any ridge has been disputed (Olive et al., 2015). Changes in hydrothermal emissions recorded in marine sediment cores flanking the East Pacific Rise also support an influence of sea level variability on ridge volcanism (Lund and Asimow, 2011; Lund et al., 2016).

4

HL09 reasoned that anti-phased pressure anomalies would cause marine volcanic anomalies to partially offset CO_2 emissions from land, but this reasoning neglected differing response times. On land, magma generally ascends rapidly from crustal magma chambers prior to eruption (Rutherford and Gardner, 2000), with ascent rates of approximately 2 km per day estimated for eruptions in Yellowstone and Mono (e.g. Befus et al., 2015). Furthermore, explosive subaerial eruptions emit CO_2 dissolved in the magma directly into the atmosphere. In contrast, volcanism at marine ridges is thought to involve much slower ascent rates, estimated to be on the order 1 km per thousand years on the basis of chemical systematics and experimental estimates (Kelemen et al., 1997; Miller et al., 2014). This slow ascent implies melt anomalies induced by sea level variations require a substantial portion of a glacial cycle to ascend to the ridge axis (Lund and Asimow, 2011). Furthermore, anomalies in CO_2 emissions involve a kind maximized delay because CO_2 partitions into initial melts and must traverse the entire melt column prior to emission (Burley and Katz, 2015).

Delays between sea level forcing and ridge emissions indicate that ridge CO_2 fluxes do not simply counteract arc emissions and opens the possibility for a system to become intrinsically oscillatory (e.g. Suarez and Schopf, 1988; Rial and Anaclerio, 2000). Here we consider the possibility that coupling amongst glaciation, volcanism, and emissions of CO_2 constitute such a delayed oscillator.

2. Model

2.1. Equations

We seek a minimalistic representation of a glacial-CO_2 oscillator involving ice volume, temperature, and atmospheric CO_2. Three equations are posited,

$$V' = -\beta T - \nu V^3, \tag{1}$$

$$T = \lambda C + fT + aF, \tag{2}$$

$$C' = (\gamma_1 - \gamma_2)V' + \gamma_3 V'(t - \delta) + \gamma_4 T'. \tag{3}$$

The rate of change of ice volume, V', is determined according to sensitivity to temperature, β, and and a bounding term, ν, representing a minimum associated with loss of all

ice and a maximum associated with finite high-latitude continental area. Temperature is determined as a function of the greenhouse effect of atmospheric CO_2 concentrations, λ, and feedbacks upon changes in temperature, f. Time required for temperature to equilibrate, for example, because of the thermal capacity of the oceans, is ignored on the basis of being short relative to the glacial-interglacial time scales of primary interest. A forcing term, F, represents the influence of changes in Earth's orbital configuration upon temperature.

Atmospheric CO_2 concentration, C, is assumed to change in proportion to changes in ice volume, sea level, and temperature. In particular, deglaciation is associated with regrowth of the biosphere, a negative feedback parameterized by γ_1, and increased emissions of CO_2 by subaerial volcanoes, a positive feedback represented by γ_2. Rising sea level decreases CO_2 emissions from mid-ocean ridges, γ_3, but with a delay of δ ky. Sea level is not explicitly represented, but ignoring hypsometric variations permits for representing its change as negatively proportional to ice volume. Finally, warming fluxes CO_2 from the ocean into the atmosphere, γ_4, on account of changes in solubility, stratification, and circulation (Gildor et al., 2002; Toggweiler et al., 2006). All variables are represented as anomalies from a mean value.

Substituting and grouping terms gives a single equation in V,

$$V' = \kappa_1 V - \kappa_2 V(t - \delta) - \kappa_3 F - \nu V^3. \tag{4}$$

Let ice volume sensitivity to temperature anomalies, to include amplification by feedbacks, be represented by $\kappa_o = \beta/(1 - f - \lambda\gamma_4)$. The net feedback associated with regrowth of the biosphere and subaerial volcanic emissions is then $\kappa_1 = \kappa_o\lambda(\gamma_2 - \gamma_1)$; delayed negative feedback associated with undersea volcanism is $\kappa_2 = \kappa_o\lambda\gamma_3$, and the effect of orbital forcing upon ice volume is $\kappa_3 = \kappa_o a$.

2.2. Parameterization

Eq. 4 is a toy model for illustrating potentially interesting behavior under plausible parameterization. Parameters are obviously uncertain, both because identification with specific is approximate and the magnitudes of those mechanisms are only approximately known. In this section we focus on parameterization of the carbon feedbacks

in Eq. 3 because their uncertainties are large and they constitute the novel behavior that Eq. 4 illustrates.

2.2.1. Subaerial volcanism

HL09 estimated that subaerial volcanism emits an additional 1000 to 5000 giga-tones of CO_2 (GtCO$_2$) above baseline during the deglaciation. Here we adopt a central value of 3000 GtCO$_2$, consistent with a quadrupling of moden global subaerial emission of $\sim$0.1 GtCO$_2$/yr (e.g. Dasgupta and Hirschmann, 2010) over the course of a 10ky deglaciation. The amount of carbon that remains in the atmosphere on ten-thousand-year timescales is uncertain, but the mid-range value adopted by HL09 of 12.5% is consistent with results from earth system models (Archer et al., 2009). Emissions of 3000 GtCO$_2$ above background levels would then give a 50 ppm rise in atmospheric CO_2. Using round numbers, the subaerial volcanic response to deglaciation is $\gamma_2 = 0.5$ ppm of atmospheric CO_2 per meter of sea level equivalent change in ice volume (ppm/msle). Model results using a lower feedback strength for subaerial volcanism, in keeping with other estimates (Watt et al., 2012; Brown et al., 2014), are discussed in Section 4.1.

2.3. Marine volcanism

The magnitude and time scale of ridge emissions in response to sea level variability is highly uncertain, largely because of the wide range of plausible values for mantle permeability. Burley and Katz (2015) consider permeability values ranging between 10^{-11}m^2 to 10^{-13}m^2 for which average delays across ridges vary from 50 ky to 200 ky. Lower permeability also accentuates differences in mantle ascent timescales across different ridge systems, leading to a greater spread in delayed response. We assume the larger 10^{-11}m^2 permeability values because they are consistent with centrifugal experiments implying a permeability of mid-ocean ridge basalts of 10^{-10}–10^{-12}m^2(Connolly et al., 2009). Also, values of permeability represented in the simple mantle melt model used by Burley and Katz (2015) should be multiplied by approximately 3.5 to bring them into consistency with the more sophisticated two-phase melt model presented by Crowley et al. (2015) as well as the simpler model presented in that paper (R. Katz personal communication), further supporting our focus on results

175 having larger permeability values.

Using ridge spreading rates weighted according to their distribution across the globe and assuming a mantle permeability of 10^{-11}m^2, Burley and Katz (2015) estimate that a 100 m drop in sea level leads to a roughly triangular pulse in emissions that occurs 50 ± 30 ky later and peaks at 6% above baseline emissions. Suppressing a
180 baseline 0.125 $GtCO_2$/yr (e.g. Dasgupta and Hirschmann, 2010) by an average of 3% over 60 ky implies a 225 $GtCO_2$ reduction in emissions and a delayed negative feedback of $\gamma_3 = -0.04$ ppm/msle, after accounting for the airborne fraction. Although γ_3 is small, it will be shown to profoundly influence the dynamics of the glacial cycles expressed by Eq. 4.

185 *2.3.1. Terrestrial carbon storage*

Carbon storage on land apparently increases from the glacial to Holocene on account of some combination of warming, increased precipitation, opening of land area other than on continental shelves, and CO_2 fertilization (Kaplan et al., 2002; Prentice et al., 2011; Ciais et al., 2012). Average ocean changes in $\delta^{13}C$ permit for quantify-
190 ing changes in terrestrial carbon because plants discriminates against ^{13}C when fixing carbon (Schackleton, 1977). Peterson et al. (2014) estimate that oceanic dissolved inorganic carbon increased, on average, by 0.34 ± 0.19 between the glacial and Holocene and Gebbie et al. (2015) estimate a 0.32 ± 0.20 increase (2σ reported uncertainty), both of which are consistent with foregoing estimates (Duplessy et al., 1988; Curry et al.,
195 1988; Tagliabue et al., 2009). Following Schackleton (1977), a 0.33‰ increase in $\delta^{13}C$ suggests that the terrestrial carbon pool increased by 500 GtC, assuming that terrestrial carbon is depleted by -25‰ and an ocean reservoir of 38,000 GtC. Ciais et al. (2012) interpret this ocean $\delta^{13}C$ in the context of increased atmospheric carbon coming out of the glacial and changes in terrestrial and atmospheric $\delta^{13}C$ compostions using a
200 three box model and estimate terrestrial regrowth of 330 GtC $\pm$800 GtC. (Uncertainty is assigned by propagating other values reported by Ciais et al. (2012).)

Another method for estimating increased terrestrial carbon storage is to infer changes in biomes from pollen data and convert these into inventories of carbon stock. Crowley (1995) estimate increased carbon storage of 750–1050 GtC between the glacial

8

and Holocene, and Adams and Faure (1998) also incorporated paleozoological data to estimate a 750–1500 GtC increase. The larger glacial-to-Holocene increase in terrestrial carbon storage inferred from biome inventories than from whole-ocean changes in δ^{13}C can be interpreted to indicate the presence of large terrestrial carbon pools during the glacial, possibly in tundra or cold steppe reservoirs (Crowley, 1995; Ciais et al., 2012), though the presence of such a pool is not required given uncertainties.

Here we prescribe a net terrestrial carbon sink of 700 GtC, straddling the marine and biome estimates, and implying that the negative feedback represented by γ_1 in Eq. 3 is 0.4 ppm/msle. Terrestrial carbon storage is made to negatively vary with ice volume, consistent with a simulation showing that the greatest increases in storage occur in the vicinity of formerly glaciated regions (Kaplan et al., 2002). Note that including our prescribed subaerial and marine volcanic sources in the three-box model of (Ciais et al., 2012) has little effect on the inferred regrowth of the biosphere because volcanic δ^{13}C is, necessarily, near the average composition of the ocean-atmosphere-terrestrial system (Sano and Williams, 1996).

2.3.2. Other possible feedbacks

A number of other potentially important carbon cycle feedbacks associated with the solid earth have not been explicitly accounted for. Glacial variations may change rates of geochemical weathering on land with consequence for rates of atmospheric CO_2 sequestration within marine sediments. If such changes are assumed concurrent with glaciation, they would be parameterized analogously with terrestrial carbon uptake, though competing influences of cooler temperature and increased rates of glacial erosion, amongst other factors, make the net effect of uncertain sign (Kump and Alley, 1994). Also notable in this context is that increased rates of arc magmatism during deglaciation could increase rates of weathering of fresh bassalts following deglaciation and contribute to drawdown of CO_2 within interglacials.

Weathering of marine crust plays a major role in carbon uptake, with estimates of crustal sequestration (Alt and Teagle, 1999) comparable to that for sediments (Plank and Langmuir, 1998). However, the majority of crustal carbon uptake occurs over time scales of tens-of-millions of years or longer (Gillis and Coogan, 2011), thus having lit-

tle influence at glacial-interglacial time scales. Hydrothermal systems near ridges may, however, respond more rapidly, possibly through alteration of crustal heat flux. Sansone et al. (1998) estimated an upper bound on the global uptake of CO_2 by near-ridge hydrothermal systems amounting to 3–8% of our assumed ridge emission rates. Assuming that variations in ridge carbon uptake do not greatly exceed the $\sim$10% changes in melt generation resulting from glacial cycles (Crowley et al., 2015) suggests that hydrothermal feedbacks are less than 1% of total emissions.

Other potential feedbacks include that deglaciation could increase ocean carbon sequestration through greater ash fertilization from subaerial volcanism (Frogner et al., 2001). Or sea level variability could influence biological carbon sequestration through changes in the amount of soluble iron emitted from ridges (Tagliabue et al., 2010). Although these more speculative processes are not specifically represented, their inclusion could generally be accommodated without changing the model formulation because of the model's simplicity and generic nature of its parameters. Indeed, the simplicity of the model fits with the uncertainty of the processes at play.

All model parameters are listed in Table 1 and combine to give a fast feedback of $\kappa_1 = 0.3$ ky^{-1}, a 50 ky delayed feedback with magnitude $\kappa_2 = 0.12$ ky^{-1}, and forcing $\kappa_3 = 3$msle/$^\circ$obliquity. These values are adopted as the default parameters for the model unless specifically noted otherwise. Sensitivity of model results to alternate parameter selection is discussed in Section 4.1.

3. Results

In order to more clearly illustrate dynamics, model behavior is examined first in the absence of forcing, then in response to sinusoidal forcing, and finally in response to the time series of obliquity variations. Although both climatic precession and obliquity influence glacial variability (Hays et al., 1976), further runs also including precession forcing do not exhibit notably different behavior and are not remarked upon further.

10

variables	value	units	description
V	—	msle	meter sea level equivalent ice volume anomaly
T	—	°C	temperature anomaly
C	—	ppm	CO_2 concentration anomaly
constants	value	units	description
δ	50	ky	mid-ocean ridge delay
ν	$1/20.55^3$	$1/\text{msle}^3$	ice volume scale
f	0.80	°C/°C	fast feedback sensitivity
β	12	msle/(ky °C)	V sensitivity to T
λ	0.01	°C/ppm	T sensitivity to C
a	0.01	°C/(°obliquity)	T sensitivity to orbital forcing
γ_1	0.4	ppm/msle	terrestrial C sensitivity to V
γ_2	0.5	ppm/msle	volcanic C sensitivity to V
γ_3	0.04	ppm/msle	volcanic C sensitivity to delayed V
γ_4	16	ppm/°C	marine C sensitivity to T
grouped constants	value	units	description
κ_1	0.30	1/ky	fast feedback sensitivity
κ_2	0.12	1/ky	delayed feedback sensitivity
κ_3	3	msle/(ky °obliquity)	V sensitivity to orbital forcing

Table 1: Variables and constants associated with the simple glacial-volcano model. Indicated values are used in all calculations except where explicitly noted otherwise.

3.1. Idealized scenarios

3.1.1. Unforced

Setting κ_3 equal to zero in Eq. 4 suppresses the forcing, and gives an equation of the form considered by Suarez and Schopf (1988) in the context of the El Niño Southern Oscillation. This unforced version of Eq. 4 has an unstable stationary point at $V = 0$ and stable stationary states at $V = \pm((\kappa_1 - \kappa_2)/\nu)^{1/2}$, given $\kappa_1 \geq \kappa_2$. Using the default parameters (Table 1) leads to model ice volume converging to one of the two stable stationary points, or remaining zero if initialized at this unstable stationary point (Fig. 1a). Similar results hold when setting κ_1 to 0.5 ky^{-1} (Fig. 1).

If the stationary fixed points are brought closer together by specifying κ_1 equal to 0.2, the delayed feedback generates oscillations with a period of slightly greater than 100 ky (Fig. 1c). Qualitatively, oscillations occur when the delayed negative feedback is of sufficient strength to drive the system away from one stable stationary state toward the other, where the requisite magnitude depends upon the other parameters (Suarez and Schopf, 1988). Oscillation periods are always greater than two times δ, reflecting the delay in the term driving transitions between otherwise stable states and the time required to transition between states. Note that Rial and Anaclerio (2000) also considered a delay differential equations in the context of the Late Pleistocene glacial cycles, though the physical origins of the delay were unclear.

3.1.2. Periodic forcing and phase locking

More relevant to Pleistocene glacial-interglacial variations is a case where Eq. 4 is driven by changes in Earth's orbital configuration. In this case, an idealized sinusoidal version of obliquity forcing is used with a 41 ky period and variance equivalent to that of obliquity over the last 2 million years. Specifying κ_1 equal to 0.5, the system cycles with the same 41ky period as the forcing about one of the two stable states identified in the unforced scenario (Fig. 1b), depending on initial ice volume and the phase of the forcing. With κ_1 set to a smaller value of 0.2, the delayed negative feedback interacts with the orbital forcing to produce larger oscillations with a 123 ky period, or three obliquity cycles (Fig. 1d). In this case, the forcing excites a nonlinear response

12

with a time scale reflecting the combined influences of the orbital-forcing and delayed-oscillator periods (c.f., Fig. 1c,d).

The forced system is phase locked in the sense that the forcing and model maintain a consistent phase relationship. A system is linearly phase locked when the forcing and response have equal periods, and nonlinearly phase locked when forcing period and model response are in integer ratios. Classic examples of phase locking are that two pendulum clocks suspended from a single beam can become linearly phase locked with one another on account of slight motions of the beam (Huygens, 1986) and that the orbital periods of Pluto and Neptune are nonlinearly phase locked in a ratio of three to two (Malhotra, 1994). Another demonstration that the model response is phase locked to the forcing comes from the fact that solutions converge onto one of two common trajectories for any initial condition (Fig. 1b,d). See Pikovsky et al. (2003) for a general discussion of phase locking.

Nonlinear phase locking of the model response to orbital forcing is consistent with observational tests that indicate late-Pleistocene glacial cycles are nonlinearly phase locked to obliquity (Huybers and Wunsch, 2005), where the ratio of periods is one glacial cycle to two or three obliquity cycles. Simulations including a precession period also produce phase locking to this higher frequency variability, also consistent with observations (Huybers, 2011). Variations in eccentricity also appear to be phase locked with late-Pleistocene glacial cycles (Lisiecki, 2010) and may contribute to setting the 100 ky timescale, but here we focus on illustrating that the 100 ky timescale can be generated internally. Such internal generation of 100 ky variability is consistent with the fact that the largest deglaciation of the Pleistocene occurred despite sustained low values of eccentricity (Maslin and Brierley, 2015, e.g.).

Most models of Late Pleistocene glacial cycles posit phase locking between orbital variations and Pleistocene glacial cycles (Tziperman et al., 2006; Crucifix, 2013). An important requirement for a system to exhibit nonlinear phase locking is the presence of a response time scale internal to the system in the vicinity of $\sim$100 ky. Previous studies have generally assumed that a 100 ky time scale is intrinsic to the build-up and collapse of ice sheets (Imbrie and Imbrie, 1980), possibly including contributions from isostatic compensation of the lithosphere (Oerlemans, 1980), or to changes in the

13

carbon chemistry of the oceans (Toggweiler, 2008). To our knowledge, this is the first model to explore the interaction of glaciation and volcanism in generating a ∼100 ky response time scale.

3.1.3. State dependence

Assigning κ_1 equal to 0.3ky^{-1} evokes a state dependence in which the period and amplitude of the model response depends upon the initial condition. For example, model runs initiated near an equilibrium values of ± 35 msle undergo small amplitude 41 ky oscillations analogous to those found with $\kappa_1 = 0.5\text{ky}^{-1}$ (Fig. 1f). Runs initialized far from equilibrium, however, undergo large-amplitude and long-period oscillations similar to those found with $\kappa_1 = 0.2\text{ky}^{-1}$. Interestingly, whereas the solution with $\kappa_1 = 0.2\text{ky}^{-1}$ exhibits 3 to 1 phase locking, the period of the large-amplitude solution with $\kappa_1 = 0.3\text{ky}^{-1}$ has a period of ∼127.1 ky. No low-order integer ratio exists between the forcing and model response periods, indicating that the model trajectory no longer repeats. Instead of a limit cycle, the model response follows a so-called limit torus defined by incommensurate forcing and response periods. Trajectories are non-chaotic, however, because those initialized near one another tend to converge over time. Trials with a wide range of other parameters also failed to indicate the divergence of model trajectories that is the hallmark of chaos. See Mitsui et al. (2015) for discussion of another glacial model exhibiting non-chaotic and limit-torus behavior.

Despite not repeating and having an incommensurate forcing and response period, model glacial cycles typically maintain phase locking. For example, in a 5 million run of the model, 90% of the downward zero-crossings of ice volume anomalies occur after three obliquity cycles to within $\pm 45°$. The overall longer period arises because in rare cases model glacial cycles span four, instead of three, obliquity cycles. For these longer glacial cycles, phase-locking is generally temporarily lost.

Another view of the model response is provided by plotting ice volume against CO_2 (Fig. 2). The two stable fixed points found for the unforced model become attractors in the forced version, and if the model is initialized near an attractor, its trajectory converges onto a stable limit cycle around one of the attractors with a period of 41 ky. If initialized further from an attractor, the model trajectory encompasses both the pos-

14

itive and negative ice volume attractors in larger-amplitude and longer-period glacial cycles. State dependence arises from the delayed feedback term introducing different magnitude perturbations dependent on foregoing ice volume anomalies, and suggests that the system is capable of transitioning between different oscillatory regimes.

3.2. Full obliquity forcing

As a final level of complexity, the model is driven by anomalies in obliquity variations (Laskar et al., 2004). Obliquity cycle amplitudes range from $0.34°$ to $1.26°$ over the last 2 Ma, as determined using a complex demodulation. Initializing the model at 2 Ma with an ice volume of -35 msle leads to a trajectory initially having small-amplitude 41 ky glacial cycles that transition toward larger-amplitude and longer-period glacial cycles around 1.1 Ma. In phase space, the model initially orbits the small ice volume attractor before escaping into a larger amplitude orbit that encompasses both attractors (Fig. 3). The stages of the model response are considered in more detail below. Note that although the model is not itself chaotic, Earth's orbital configuration is chaotic (Laskar et al., 2004), and this fully-forced simulation inherits chaotic qualities.

3.2.1. 40 ky Early Pleistocene variability

During the Early Pleistocene (from 2–1 Ma), model glacial cycles oscillate at 41 ky periods in the range of -35 ± 10 msle, where negative values denote less ice volume and higher sea level relative to the Late-Pleistocene average. Temperature ranges over $0.5\pm0.5°C$ (Fig. 3). Both ice volume and temperature variations are smaller than indicated by early Pleistocene observational estimates by roughly a factor of two (Elderfield et al., 2012; Rohling et al., 2014). CO_2 ranges over 10 ± 10 ppm, which is also small relative to a recent reconstruction (Martínez-Botí et al., 2015), though orbital-scale amplitudes remain uncertain.

Model ice volume lags the obliquity forcing by $24°$, on average, though nonlinearities in the response create phase anomalies with ice volume leading by as much as $40°$ at 1.74 Ma, when obliquity has an anomalously small amplitude, and lagging by as much $95°$ at 1.45 Ma, when obliquity has an anomalously large amplitude (Fig. 4a,b). Model variations in the phasing of the response relative to forcing imply that the com-

15

mon practice of estimating age through tuning a chronology to maintain a constant phase with orbital forcing may entail substantial timing errors, in this case of as much as ± 7 ky. These uncertainties are, of course, in addition to others inherent to aligning sub-sampled sequences containing noise to a putative forcing signal (e.g. Proistosescu et al., 2012).

3.2.2. Mid-Pleistocene Transition

Previous studies have largely focussed on the Mid-Pleistocene Transition (MPT) as resulting from changes in boundary conditions, including glacial scouring of sediments increasing the frictional coupling of Laurentian glaciation with bedrock (Clark et al., 2006) or decreases in background atmospheric CO_2 concentrations activating new sources of variability (Raymo et al., 1997; Berger et al., 1999; Raymo et al., 2006). In this simulation (Fig. 3a,b), 41 ky glacial cycles are perturbed by a string of large-amplitude obliquity cycles beginning near 1.4 Ma and ultimately transition toward larger-amplitude and longer-period glacial cycles at 1.1 Ma.

The model MPT occurs within the 1.25–0.70 Ma interval identified by Clark et al. (2006), but the appearance of a progression in glacial statistics toward greater amplitude, longer period, and more asymmetric oscillations (Huybers, 2007) is not captured. Instead, the transition is sharp, spanning a single orbital cycle, as found by Elderfield et al. (2012) on the basis of records from individual marine sediment cores. A running spectral estimate of the model time series demonstrates a transition from variability dominated by 41 ky periods to one near 100 ky periods (Fig. 3c). Additional concentrations of energy exist at harmonics of the forcing and response periods that are introduced through model nonlinearities, for example, near frequencies of 2/41ky. The evolution of spectral properties also include the appearance of excess low frequency variability centered at about 1.4 Ma that is coincident with larger amplitude obliquity cycles (Fig. 3d,e).

Obliquity modulations control MPT timing in the sense that a constant amplitude forcing produces no such transition in the model (e.g., Fig. 1f), but it is a form of threshold crossing that is also sensitive to other changes in model specification. Sensitivity to small changes in model parameters or forcing indicates, on the one hand, that transition

timing could be effectively stochastic (Crucifix, 2013) and, on the other, that difficulty in identifying a specific orbital configuration associated with the mid-Pleistocene Transition (e.g. Berger et al., 1999; Clark et al., 2006) does not necessarily rule out orbital variation as the underlying cause of the transition.

Other simple mathematical models have been proposed containing spontaneous MPT-like events (Saltzman and Verbitsky, 1993; Huybers, 2009), though these tended to exhibit multiple transitions between 41 ky and $\sim$100 ky oscillatory regimes, seemingly difficult to reconcile with the long strings of 40 ky glacial cycles observed during the Early Pleistocene. Long integrations of Eq. 4, however, demonstrate a singular transition from early- to late-Pleistocene style glaciations, at least using the parameters in Table 1.

3.2.3. 100 ky Late Pleistocene variability

After the MPT, glacial cycles are characterized by anomalies in sea level ranging between 0 ± 60 msle, CO_2 between 0 ± 40ppm, and temperature of $0 \pm 2°C$. These amplitude are roughly consistent with magnitudes of glacial-interglacial variability inferred from models and coral records (Lambeck et al., 2014), CO_2 variations found in ice core measurements (Petit et al., 1999), and global temperature changes inferred from models (Schneider von Deimling et al., 2006) and observations (Elderfield et al., 2012). Although model glacial cycles typically span just over three obliquity cycles, ranging from 124 ky to 132 ky, two cycles are approximately 150 ky and excede those observed for late Pleistocene glacial cycles.

Temperature and CO_2 variations are closely in phase with one another because of strong linear coupling (Eqs. 2,3), but influences from orbital forcing and ice volume cause temperature to lead CO_2 by as much as 400 years during deglaciations (Fig. 4c,d). Model temperature leads CO_2 because it is directly influenced by orbital forcing, whereas CO_2 is indirectly influenced by orbital variations through a slow ice volume response. Although the degree to which model temperature can be equated with regional variations in Antarctica is questionable, these results are roughly consistent with Antarctic ice core studies, being somewhat smaller than the 800 ± 200 lead estimated by Caillon et al. (2003) for termination three and somewhat larger than es-

17

timates by Pedro et al. (2012) and Parrenin et al. (2013) for most portions of the last deglaciation.

4. Further discussion and conclusion

The model is rather simplistic. Absence of cryosphere, ocean-atmosphere, and ridge and arc dynamics, as well as lack of carbon chemistry, make it at best a toy capable of illustrating certain features of glacial cycle dynamics. Foremost, the model illustrates that a delayed negative feedback may have an important influence upon the dynamics of glacial cycles, potentially accounting for the transition to $\sim$100 ky oscillations during the late Pleistocene. In considering the plausibility of this model for explaining Late Pleistocene glacial cycles, it useful to further consider its sensitivity to different choices of parameters and how it might be further tested.

4.1. Parameter sensitivity

Characterizing the sensitivity of the model to changes in parameters is relevant both from the perspective of stability and plausibility with respect to observations. The metric focussed on is the dominant period of variability, assessed as the most energetic Fourier component in 2 Ma integrations of the model. Sinusoidal forcing is adopted in order to obtain a more uniform time scale of response. Note that this period can differ from the interval over which the system repeats because of the potential for minor alterations in features of an oscillation, or instances of atypically short or long cycles.

The model period is sensitive to plausible changes in the magnitude and delay associated with κ_2. Increasing the magnitude of κ_2 and decreasing the delay generally leads to shorter period oscillations, with a sharp transition between 41 ky and longer-period glacial cycles that is primarily controlled by κ_2. There are also longer but still discrete steps within the longer-period regime that are more sensitive to the delay (Fig. 5a).

The model could be brought into a regime with 100 ky glacial cycles, for example, by increasing κ_2 from 0.12 ky^{-1} to 0.17 ky^{-1} and decreasing δ from 50 ky to 40 ky. Although values adopted herein are restricted to those explicitly considered by (Burley and Katz, 2015), extrapolation from their sensitivity studies indicate that increasing the

18

10^{-11} m^2 mantle permeability by less than an order of magnitude would generate ridge feedbacks resulting in 100 ky glacial cycles. Such values would still be consistent with experimentally estimated values of permeability (Connolly et al., 2009; Miller et al., 2014).

A similar assessment of model sensitivity to varying κ_1 and κ_2 indicates that increasing κ_1 leads to decreases in period, but that all values of κ_1 and κ_2 give glacial cycles that are somewhat longer than 100 ky when other parameters are held constant (Fig. 5b). These sensitivity studies also emphasize how small volcanic feedback contributions from ridge volcanism are generally sufficient to cause the system to oscillate at periods that are multiples of the forcing.

Simulations presented so far have a single delay time, whereas delays will vary substantially according to ocean spreading rate (Burley and Katz, 2015). Assuming mantle permeability values of 10^{-11}m^2, Burley and Katz (2015) estimate that emissions would be distributed over an approximately 60 ky triangular pulse. Further analyses distributing delays triangularly between 20ky and 80ky produce similar oscillation, including similar magnitudes and retaining a transition from 41 ky to longer-period and larger-amplitude glacial cycles at about 1.1 Ma, but with the period of late-Pleistocene glacial cycles tending to increase. Consideration of distributed delays thus further indicates the importance of a smaller delay for ridge CO_2 emissions for purposes of matching observations. Alternatively, shorter time scales might emerge if the model were made more realistic, for example, through including ice dynamics that allow for rapid deglaciations.

4.2. Testability

The assumption of increased CO_2 emissions from subaerial volcanism following deglaciation is supported by previous assessments of global-scale volcanic activity (Kutterolf et al., 2013; Watt et al., 2012; Brown et al., 2014), but accurately quantifying this feedback requires further development. The relationship between regional ice unloading and changes in volcanism is only documented in detail for isolated systems (Bacon and Lanphere, 2006; Rawson et al., 2015). The seeming impossibility of comprehensively mapping volcanism over the Quaternary also points to the utility of

19

further developing methods to correct for observational bias (Deligne et al., 2010). Improved observational constraints on the relationship between eruptions and emissions of CO_2 (Cartigny et al., 2008), to include contributions from passive eruptions and intrusive emplacement of magma (Allard et al., 1994), will also aid in determining the climate significance of anomalies in volcanism. Finally, improved modeling of how surface loads influence eruption timing and composition (e.g. Geyer and Bindeman, 2011) will improve opportunities for comparing simulations against eruption data and may provide a basis for better inferring net CO_2 emission.

Similarly, the representation of a delayed CO_2 response from mid-ocean ridge volcanism is supported by sediment core records from near ridges (Lund et al., 2016), bathymetric analyses at individual ridge locations (Crowley et al., 2015), observations and models of Icelandic volcanism (Maclennan et al., 2002), and models applicable to mid-ocean ridges generally (Burley and Katz, 2015). Further development is, nonetheless, critical to constraining this potential influence upon glacial cycles. Continued analysis of ridge bathymetry and sediment core data will elucidate whether anomalies are global, how spreading rate influences magmatic response, and may help constrain mantle permeability. Also relevant are efforts to better determine the magnitude and timing of CO_2 emissions at ridges in response to sea level anomalies, to include better constraining the rate at which melt upwells at ridges (Connolly et al., 2009; Miller et al., 2014), and accounting for the influence of CO_2 concentrations on viscosity and other mantle melt characteristics beneath mid-ocean ridges (Kono et al., 2014).

The model presented here represents variations in glaciation and atmospheric CO_2 as fundamentally linked, amplifying changes through an immediate postive feedback and oscillating at 100 ky time scales because of a delayed negative feedback. The novelty of this model stems conceptually from invoking volcanic contributions from both subaerial and submarine volcanism, and dynamically from positing that late-Pleistocene glacial cycles represent a transition to delayed oscillations. Models of glacial-interglacial CO_2 variations that depend on ocean storage have been assessed in light of continuing improvement in our understanding of how carbon circulates amongst the oceans, atmosphere, and terrestrial biosphere. Similarly, it is anticipated that the volcanic processes represented in this simple model will be tested in light of

20

improved understanding of the circulation of carbon in the solid earth.

References

Adams, J.M., Faure, H., 1998. A new estimate of changing carbon storage on land since the last glacial maximum, based on global land ecosystem reconstruction. Global and Planetary Change 16, 3–24.

Allard, P., Carbonnelle, J., Metrich, N., Loyer, H., Zettwoog, P., 1994. Sulphur output and magma degassing budget of stromboli volcano. Nature 368, 326–330.

Alt, J.C., Teagle, D.A., 1999. The uptake of carbon during alteration of ocean crust. Geochimica et Cosmochimica Acta 63, 1527–1535.

Anderson, R., Ali, S., Bradtmiller, L., Nielsen, S., Fleisher, M., Anderson, B., Burckle, L., 2009. Wind-driven upwelling in the southern ocean and the deglacial rise in atmospheric co2. science 323, 1443–1448.

Archer, D., Eby, M., Brovkin, V., Ridgwell, A., Cao, L., Mikolajewicz, U., Caldeira, K., Matsumoto, K., Munhoven, G., Montenegro, A., et al., 2009. Atmospheric lifetime of fossil fuel carbon dioxide. Annual Review of Earth and Planetary Sciences 37, 117.

Arrhenius, S., 1896. On the influence of carbonic acid in the air upon the temperature of the ground. The London, Edinburgh, and Dublin Philosophical Magazine and Journal of Science 41, 237–276.

Arrhenius, S., Holden, E.S., 1897. On the influence of carbonic acid in the air upon the temperature of the earth. Publications of the Astronomical Society of the Pacific 9, 14–24.

Bacon, C.R., Lanphere, M.A., 2006. Eruptive history and geochronology of mount mazama and the crater lake region, oregon. Geological Society of America Bulletin 118, 1331–1359.

Befus, K.S., Manga, M., Gardner, J.E., Williams, M., 2015. Ascent and emplacement dynamics of obsidian lavas inferred from microlite textures. Bulletin of Volcanology 77, 1–17.

Berger, A., Li, X., Loutre, M.F., 1999. Modelling northern hemisphere ice volume over the last 3ma. Quaternary Science Reviews 18, 1–11.

Broecker, W., Clark, E., Barker, S., 2008. Near constancy of the pacific ocean surface to mid-depth radiocarbon-age difference over the last 20 kyr. Earth and Planetary Science Letters 274, 322–326.

Broecker, W.S., 2013. What Drives Glacial Cycles? Eldigio Press.

Broecker, W.S., Yu, J., Putnam, A.E., 2015. Two contributors to the glacial co_2 decline. Earth and Planetary Science Letters 429, 191–196.

Brown, S.K., Crosweller, H.S., Sparks, R.S.J., Cottrell, E., Deligne, N.I., Guerrero, N.O., Hobbs, L., Kiyosugi, K., Loughlin, S.C., Siebert, L., et al., 2014. Characterisation of the quaternary eruption record: analysis of the large magnitude explosive volcanic eruptions (lameve) database. Journal of Applied Volcanology 3, 5.

Bryson, R., Bryson, R., Ruter, A., 2006. A calibrated radiocarbon database of late quaternary volcanic eruptions. eEarth Discussions 1, 123–134.

Burley, J., Katz, R.F., 2015. Variations in mid-ocean ridge co2 emissions driven by glacial cycles. arXiv preprint arXiv:1503.02308 .

Caillon, N., Severinghaus, J.P., Jouzel, J., Barnola, J.M., Kang, J., Lipenkov, V.Y., 2003. Timing of atmospheric co2 and antarctic temperature changes across termination iii. Science 299, 1728–1731.

Cartigny, P., Pineau, F., Aubaud, C., Javoy, M., 2008. Towards a consistent mantle carbon flux estimate: Insights from volatile systematics (h 2 o/ce, δd, co 2/nb) in the north atlantic mantle (14 n and 34 n). Earth and Planetary Science Letters 265, 672–685.

22

Ciais, P., Tagliabue, A., Cuntz, M., Bopp, L., Scholze, M., Hoffmann, G., Lourantou, A., Harrison, S.P., Prentice, I., Kelley, D., et al., 2012. Large inert carbon pool in the terrestrial biosphere during the last glacial maximum. Nature Geoscience 5, 74–79.

Clark, P.U., Archer, D., Pollard, D., Blum, J.D., Rial, J.A., Brovkin, V., Mix, A.C., Pisias, N.G., Roy, M., 2006. The middle pleistocene transition: characteristics, mechanisms, and implications for long-term changes in atmospheric pco 2. Quaternary Science Reviews 25, 3150–3184.

Connolly, J.A., Schmidt, M.W., Solferino, G., Bagdassarov, N., 2009. Permeability of asthenospheric mantle and melt extraction rates at mid-ocean ridges. Nature 462, 209–212.

Crowley, J.W., Katz, R.F., Huybers, P., Langmuir, C.H., Park, S.H., 2015. Glacial cycles drive variations in the production of oceanic crust. Science 347, 1237–1240.

Crowley, T.J., 1995. Ice age terrestrial carbon changes revisited. Global Biogeochemical Cycles 9, 377–389.

Crucifix, M., 2013. Why could ice ages be unpredictable? Climate of the Past 9, 2253–2267.

Curry, W.B., Duplessy, J.C., Labeyrie, L., Shackleton, N.J., 1988. Changes in the distribution of δ13c of deep water σco2 between the last glaciation and the holocene. Paleoceanography 3, 317–341.

Dasgupta, R., Hirschmann, M.M., 2010. The deep carbon cycle and melting in earth's interior. Earth and Planetary Science Letters 298, 1–13.

Schneider von Deimling, T., Ganopolski, A., Held, H., Rahmstorf, S., 2006. How cold was the last glacial maximum? Geophysical Research Letters 33.

Deligne, N., Coles, S., Sparks, R., 2010. Recurrence rates of large explosive volcanic eruptions. Journal of Geophysical Research: Solid Earth (1978–2012) 115.

Doughty, A.M., Schaefer, J.M., Putnam, A.E., Denton, G.H., Kaplan, M.R., Barrell, D.J., Andersen, B.G., Kelley, S.E., Finkel, R.C., Schwartz, R., 2015. Mismatch of

23

glacier extent and summer insolation in southern hemisphere mid-latitudes. Geology 43, 407–410.

Duplessy, J., Shackleton, N., Fairbanks, R., Labeyrie, L., Oppo, D., Kallel, N., 1988. Deepwater source variations during the last climatic cycle and their impact on the global deepwater circulation. Paleoceanography 3, 343–360.

Elderfield, H., Ferretti, P., Greaves, M., Crowhurst, S., McCave, I., Hodell, D., Piotrowski, A., 2012. Evolution of ocean temperature and ice volume through the mid-pleistocene climate transition. Science 337, 704–709.

Ferrari, R., Jansen, M.F., Adkins, J.F., Burke, A., Stewart, A.L., Thompson, A.F., 2014. Antarctic sea ice control on ocean circulation in present and glacial climates. Proceedings of the National Academy of Sciences 111, 8753–8758.

Frogner, P., Gíslason, S.R., Óskarsson, N., 2001. Fertilizing potential of volcanic ash in ocean surface water. Geology 29, 487–490.

Gebbie, G., Peterson, C.D., Lisiecki, L.E., Spero, H.J., 2015. Global-mean marine δ 13 c and its uncertainty in a glacial state estimate. Quaternary Science Reviews 125, 144–159.

Geyer, A., Bindeman, I., 2011. Glacial influence on caldera-forming eruptions. Journal of Volcanology and Geothermal Research 202, 127–142.

Gildor, H., Tziperman, E., Toggweiler, J., 2002. Sea ice switch mechanism and glacial-interglacial co2 variations. Global Biogeochemical Cycles 16, 6–1.

Gillis, K., Coogan, L., 2011. Secular variation in carbon uptake into the ocean crust. Earth and Planetary Science Letters 302, 385–392.

Hays, J., Imbrie, J., Shackleton, N., 1976. Variations in the earth's orbit: Pacemaker of the ice ages. Science (New York, NY) 194, 1121–1132.

Huybers, P., 2007. Glacial variability over the last two million years: an extended depth-derived agemodel, continuous obliquity pacing, and the pleistocene progression. Quaternary Science Reviews 26, 37–55.

24

Huybers, P., 2009. Pleistocene glacial variability as a chaotic response to obliquity forcing. Climate of the Past 5.

Huybers, P., 2011. Combined obliquity and precession pacing of late pleistocene deglaciations. Nature 480, 229–232.

Huybers, P., Langmuir, C., 2009. Feedback between deglaciation, volcanism, and atmospheric co 2. Earth and Planetary Science Letters 286, 479–491.

Huybers, P., Wunsch, C., 2005. Obliquity pacing of the late pleistocene glacial terminations. Nature 434, 491–494.

Huygens, C., 1986. The pendulum clock, 1673. Trans RJ Blackwell, The Iowa State University Press .

Imbrie, J., Imbrie, J.Z., 1980. Modeling the climatic response to orbital variations. Science 207, 943–953.

Jaccard, S., Hayes, C.T., Martínez-García, A., Hodell, D., Anderson, R.F., Sigman, D., Haug, G., 2013. Two modes of change in southern ocean productivity over the past million years. Science 339, 1419–1423.

Jellinek, A.M., Manga, M., Saar, M.O., 2004. Did melting glaciers cause volcanic eruptions in eastern california? probing the mechanics of dike formation. Journal of Geophysical Research: Solid Earth (1978–2012) 109.

Kaplan, J.O., Prentice, I.C., Knorr, W., Valdes, P.J., 2002. Modeling the dynamics of terrestrial carbon storage since the last glacial maximum. Geophysical Research Letters 29.

Kelemen, P., Hirth, G., Shimizu, N., Spiegelman, M., Dick, H., 1997. A review of melt migration processes in the adiabatically upwelling mantle beneath oceanic spreading ridges. Philosophical Transactions of the Royal Society of London A: Mathematical, Physical and Engineering Sciences 355, 283–318.

Kelly, M.A., Russell, J.M., Baber, M.B., Howley, J.A., Loomis, S.E., Zimmerman, S., Nakileza, B., Lukaye, J., 2014. Expanded glaciers during a dry and cold last glacial maximum in equatorial east africa. Geology 42, 519–522.

Kono, Y., Kenney-Benson, C., Hummer, D., Ohfuji, H., Park, C., Shen, G., Wang, Y., Kavner, A., Manning, C.E., 2014. Ultralow viscosity of carbonate melts at high pressures. Nature communications 5.

Kump, L., Alley, R.B., 1994. Global chemical weathering on glacial time scales. Material Fluxes on the Surface of the Earth , 46–60.

Kutterolf, S., Jegen, M., Mitrovica, J.X., Kwasnitschka, T., Freundt, A., Huybers, P.J., 2013. A detection of milankovitch frequencies in global volcanic activity. Geology 41, 227–230.

Lambeck, K., Rouby, H., Purcell, A., Sun, Y., Sambridge, M., 2014. Sea level and global ice volumes from the last glacial maximum to the holocene. Proceedings of the National Academy of Sciences 111, 15296–15303.

Laskar, J., Correia, A., Gastineau, M., Joutel, F., Levrard, B., Robutel, P., 2004. Long term evolution and chaotic diffusion of the insolation quantities of mars. Icarus 170, 343–364.

Lee, S.Y., Chiang, J.C., Matsumoto, K., Tokos, K.S., 2011. Southern ocean wind response to north atlantic cooling and the rise in atmospheric co2: Modeling perspective and paleoceanographic implications. Paleoceanography 26.

Licciardi, J.M., Kurz, M.D., Curtice, J.M., 2007. Glacial and volcanic history of icelandic table mountains from cosmogenic 3 he exposure ages. Quaternary Science Reviews 26, 1529–1546.

Lisiecki, L.E., 2010. Links between eccentricity forcing and the 100,000-year glacial cycle. Nature geoscience 3, 349–352.

Lund, D., Asimow, P., Farley, K., Rooney, T., Seeley, E., Jackson, E., Durham, Z., 2016. Enhanced east pacific rise hydrothermal activity during the last two glacial terminations. Science 351, 478–482.

Lund, D.C., 2013. Deep pacific ventilation ages during the last deglaciation: Evaluating the influence of diffusive mixing and source region reservoir age. Earth and Planetary Science Letters 381, 52–62.

Lund, D.C., Asimow, P.D., 2011. Does sea level influence mid-ocean ridge magmatism on milankovitch timescales? Geochemistry, Geophysics, Geosystems 12.

Maclennan, J., Jull, M., McKenzie, D., Slater, L., Grönvold, K., 2002. The link between volcanism and deglaciation in iceland. Geochemistry, Geophysics, Geosystems 3, 1–25.

Malhotra, R., 1994. Nonlinear resonances in the solar system. Physica D: Nonlinear Phenomena 77, 289–304.

Manabe, S., Broccoli, A., 1985. The influence of continental ice sheets on the climate of an ice age. J. geophys. Res 90, 2167–2190.

Martínez-Botí, M., Foster, G., Chalk, T., Rohling, E., Sexton, P., Lunt, D., Pancost, R., Badger, M., Schmidt, D., 2015. Plio-pleistocene climate sensitivity evaluated using high-resolution co2 records. Nature 518, 49–54.

Martínez-García, A., Sigman, D.M., Ren, H., Anderson, R.F., Straub, M., Hodell, D.A., Jaccard, S.L., Eglinton, T.I., Haug, G.H., 2014. Iron fertilization of the subantarctic ocean during the last ice age. Science 343, 1347–1350.

Maslin, M.A., Brierley, C.M., 2015. The role of orbital forcing in the early middle pleistocene transition. Quaternary International .

Mekik, F.A., Anderson, R.F., Loubere, P., François, R., Richaud, M., 2012. The mystery of the missing deglacial carbonate preservation maximum. Quaternary Science Reviews 39, 60–72.

Miller, K.J., Zhu, W.l., Montési, L.G., Gaetani, G.A., 2014. Experimental quantification of permeability of partially molten mantle rock. Earth and Planetary Science Letters 388, 273–282.

27

Mitsui, T., Crucifix, M., Aihara, K., 2015. Bifurcations and strange nonchaotic attractors in a phase oscillator model of glacial–interglacial cycles. Physica D: Nonlinear Phenomena 306, 25–33.

Nowell, D.A., Jones, M.C., Pyle, D.M., 2006. Episodic quaternary volcanism in france and germany. Journal of Quaternary Science 21, 645–675.

Oerlemans, J., 1980. Model experiments on the 100, 000-yr glacial cycle. Nature 287, 430–432.

Olive, J.A., Behn, M.D., Ito, G., Buck, W.R., Escartín, J., Howell, S., 2015. Sensitivity of seafloor bathymetry to climate-driven fluctuations in mid-ocean ridge magma supply. Science 350, 310–313.

Parrenin, F., Masson-Delmotte, V., Köhler, P., Raynaud, D., Paillard, D., Schwander, J., Barbante, C., Landais, A., Wegner, A., Jouzel, J., 2013. Synchronous change of atmospheric co2 and antarctic temperature during the last deglacial warming. Science 339, 1060–1063.

Pedro, J.B., Rasmussen, S.O., van Ommen, T.D., 2012. Tightened constraints on the time-lag between antarctic temperature and co 2 during the last deglaciation. Climate of the Past 8, 1213–1221.

Peterson, C.D., Lisiecki, L.E., Stern, J.V., 2014. Deglacial whole-ocean δ13c change estimated from 480 benthic foraminiferal records. Paleoceanography 29, 549–563.

Petit, J.R., Jouzel, J., Raynaud, D., Barkov, N.I., Barnola, J.M., Basile, I., Bender, M., Chappellaz, J., Davis, M., Delaygue, G., et al., 1999. Climate and atmospheric history of the past 420,000 years from the vostok ice core, antarctica. Nature 399, 429–436.

Pikovsky, A., Rosenblum, M., Kurths, J., 2003. Synchronization: a universal concept in nonlinear sciences. volume 12. Cambridge university press.

Plank, T., Langmuir, C.H., 1998. The chemical composition of subducting sediment and its consequences for the crust and mantle. Chemical geology 145, 325–394.

28

Prentice, I., Harrison, S., Bartlein, P., 2011. Global vegetation and terrestrial carbon cycle changes after the last ice age. New Phytologist 189, 988–998.

Proistosescu, C., Huybers, P., Maloof, A.C., 2012. To tune or not to tune: Detecting orbital variability in oligo-miocene climate records. Earth and Planetary Science Letters 325, 100–107.

Putnam, A.E., Schaefer, J.M., Denton, G.H., Barrell, D.J., Birkel, S.D., Andersen, B.G., Kaplan, M.R., Finkel, R.C., Schwartz, R., Doughty, A.M., 2013. the last glacial maximum at 44 s documented by a 10 be moraine chronology at lake ohau, southern alps of new zealand. Quaternary Science Reviews 62, 114–141.

Rawson, H., Naranjo, J.A., Smith, V., Fontijn, K., Pyle, D.M., Mather, T.A., Moreno, H., 2015. The frequency and magnitude of post-glacial explosive eruptions at volcán mocho-choshuenco, southern chile. Journal of Volcanology and Geothermal Research .

Rawson, H., Pyle, D.M., Mather, T.A., Smith, V.C., Fontijn, K., Lachowycz, S.M., Naranjo, J.A., 2016. The magmatic and eruptive response of arc volcanoes to deglaciation: Insights from southern chile. Geology , G37504–1.

Raymo, M., Lisiecki, L., Nisancioglu, K.H., 2006. Plio-pleistocene ice volume, antarctic climate, and the global δ18o record. Science 313, 492–495.

Raymo, M., Oppo, D., Curry, W., 1997. The mid-pleistocene climate transition: A deep sea carbon isotopic perspective. Paleoceanography 12, 546–559.

Rial, J., Anaclerio, C., 2000. Understanding nonlinear responses of the climate system to orbital forcing. Quaternary Science Reviews 19, 1709–1722.

Rohling, E., Foster, G., Grant, K., Marino, G., Roberts, A., Tamisiea, M., Williams, F., 2014. Sea-level and deep-sea-temperature variability over the past 5.3 million years. Nature 508, 477–482.

Roth, R., Joos, F., 2012. Model limits on the role of volcanic carbon emissions in regulating glacial–interglacial co 2 variations. Earth and Planetary Science Letters 329, 141–149.

29

Rutherford, M.J., Gardner, J.E., 2000. Rates of magma ascent. Encyclopedia of volcanoes , 207–217.

Saltzman, B., Verbitsky, M.Y., 1993. Multiple instabilities and modes of glacial rhythmicity in the plio-pleistocene: a general theory of late cenozoic climatic change. Climate Dynamics 9, 1–15.

Sano, Y., Williams, S.N., 1996. Fluxes of mantle and subducted carbon along convergent plate boundaries. Geophysical Research Letters 23, 2749–2752.

Sansone, F.J., Mottl, M.J., Olson, E.J., Wheat, C.G., Lilley, M.D., 1998. Co 2-depleted fluids from mid-ocean ridge-flank hydrothermal springs. Geochimica et cosmochimica acta 62, 2247–2252.

Schackleton, N., 1977. Carbon-13 in uvigerina: Tropical rain forest history and the equatorial pacific carbonate dissolution cycle, in: The Fate of Fossil Fuel in the Oceans. Plenum, New York, pp. 401–427.

Shakun, J.D., Clark, P.U., He, F., Marcott, S.A., Mix, A.C., Liu, Z., Otto-Bliesner, B., Schmittner, A., Bard, E., 2012. Global warming preceded by increasing carbon dioxide concentrations during the last deglaciation. Nature 484, 49–54.

Siebert, L., Simkin, T., Kimberly, P., 2010. Volcanoes of the World. Univ of California Press.

Sigman, D.M., Hain, M.P., Haug, G.H., 2010. The polar ocean and glacial cycles in atmospheric co2 concentration. Nature 466, 47–55.

Suarez, M.J., Schopf, P.S., 1988. A delayed action oscillator for enso. Journal of the atmospheric Sciences 45, 3283–3287.

Tagliabue, A., Bopp, L., Dutay, J.C., Bowie, A.R., Chever, F., Jean-Baptiste, P., Bucciarelli, E., Lannuzel, D., Remenyi, T., Sarthou, G., et al., 2010. Hydrothermal contribution to the oceanic dissolved iron inventory. Nature Geoscience 3, 252–256.

Tagliabue, A., Bopp, L., Roche, D., Bouttes, N., Dutay, J.C., Alkama, R., Kageyama, M., Michel, E., Paillard, D., 2009. Quantifying the roles of ocean circulation and

795 biogeochemistry in governing ocean carbon-13 and atmospheric carbon dioxide at the last glacial maximum. Climate of the Past 5, 695–706.

Toggweiler, J., 2008. Origin of the 100,000-year timescale in antarctic temperatures and atmospheric co2. Paleoceanography 23.

Toggweiler, J., Russell, J.L., Carson, S., 2006. Midlatitude westerlies, atmospheric
800 co2, and climate change during the ice ages. Paleoceanography 21.

Tolstoy, M., 2015. Mid-ocean ridge eruptions as a climate valve. Geophysical Research Letters 42, 1346–1351.

Tziperman, E., Raymo, M.E., Huybers, P., Wunsch, C., 2006. Consequences of pacing the pleistocene 100 kyr ice ages by nonlinear phase locking to milankovitch forcing.
805 Paleoceanography 21.

Watt, S., Pyle, D., Mather, T., 2012. Towards quantifying the arc-scale and global magmatic response to deglaciation, in: AGU Fall Meeting Abstracts, p. 2016.

Yu, J., Anderson, R.F., Jin, Z., Rae, J.W., Opdyke, B.N., Eggins, S.M., 2013. Responses of the deep ocean carbonate system to carbon reorganization during the last glacial–
810 interglacial cycle. Quaternary Science Reviews 76, 39–52.
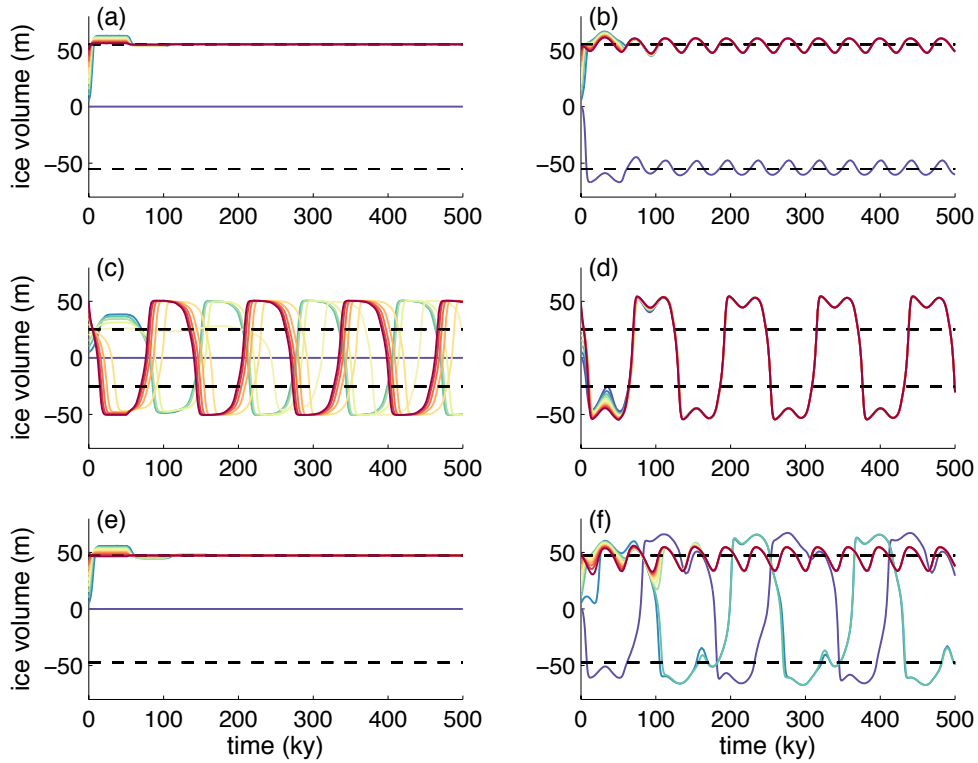
31

Figure 1: Illustrations of differing model behavior. In all cases the delayed feedback is 0.12 with the fast feedback specified as 0.5 (a,b), 0.2 (c,d), and 0.3 (e,f). The left column (a, c, e) is without forcing, and the right (b, d, f) is with 41 ky sinusoidal forcing with 0.01 amplitude. Runs are variously initialized with ice volume's evenly spaced between 0–50 msle. Large values of the fast feedback lead to solutions that are constant at model equilibrium points (a) or, with forcing (b), undergo limit cycles about an attractor. Small fast feedback values allow for delayed oscillations at a period of slightly greater than twice the delay (c) or, when including forcing (d), with a response time scale that, in this case, is slightly greater than three times the forcing period. An intermediate strength fast feedback produces a greater variety of solutions (e,f). Without forcing (e), both positive and negative solutions can be realized despite initialization all being non-negative. Runs with forcing (f) initialized at a value of 50 produce 41ky variability similar to that in panel (b), whereas runs initialized at smaller ice volume anomalies produce longer-period variability similar to those in panel (d).
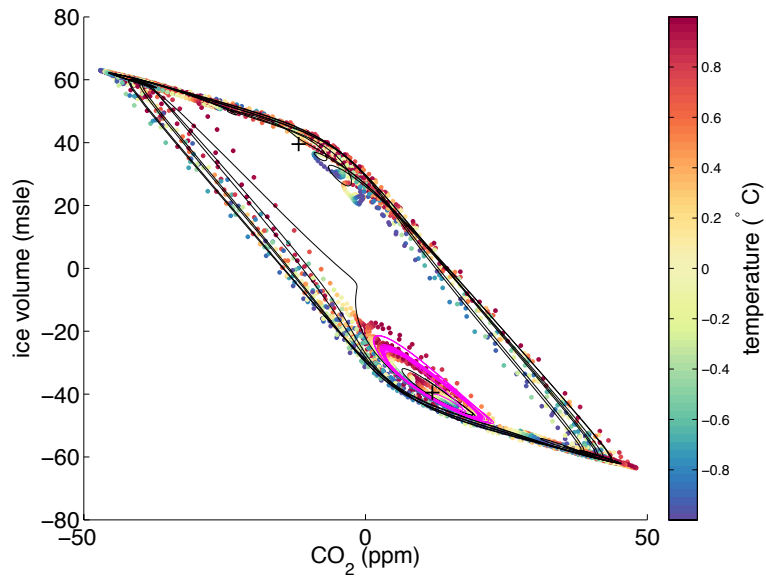
Figure 2: Limit cycles associated with model Pleistocene glacial cycles. Three different model runs are shown where the initial conditions and forcing differ. (1. Magenta curve) Using idealized periodic obliquity forcing and an initial ice volume anomaly of -35 msle the model undergoes a small limit cycles around one attractor (black cross at -40 msle, 12 ppm, and -0.6°C). (2. Black curve). Again with idealized forcing, but initializing ice volume at -40 msle the model undergoes a larger limit cycle encompassing both attractors (black crosses at ∓40 msle and ±12 ppm). (3. Dots spaced at 1 ky intervals with shading indicating temperature anomalies). Using the full obliquity variability and an initial ice volume of 20.55 msle the model initially undergoes a limit cycle near the lower attractor, but then escapes into larger oscillations around both attractors. In all cases the trajectory is counter clockwise, indicating the CO_2 leads changes in ice volume.
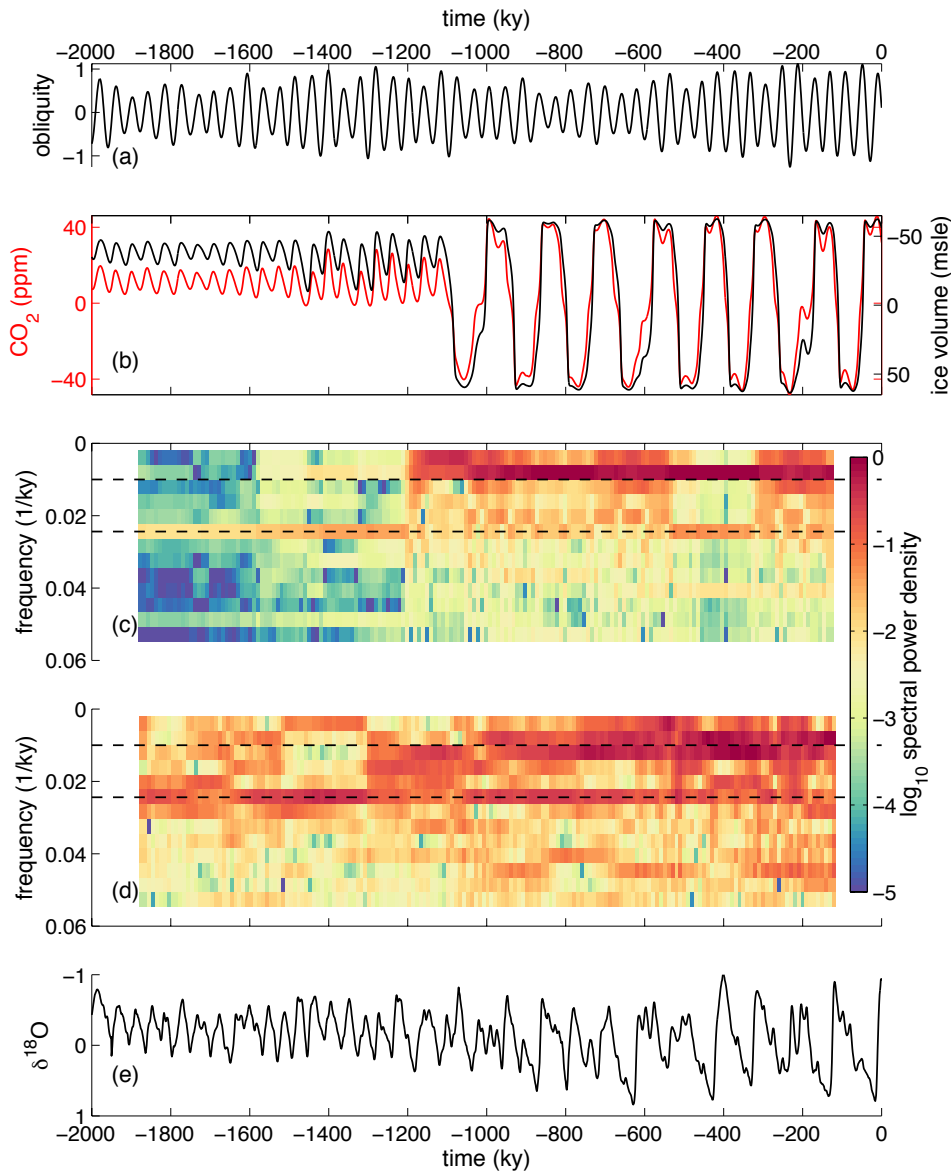
Figure 3: Mid-Pleistocene transition from obliquity forcing. **(a)** Obliquity variations (Laskar et al., 2004) are normalized to zero mean and an average amplitude of 0.3, which gives a maximum amplitude consistent with standard model parameters. **(b)** Initially the solution is trapped near the negative ice volume attractor (c.f., Fig. 1b) until a large obliquity oscillation near 1.1 Ma transitions the system to a larger-amplitude and longer-period oscillations (c.f., Fig 1d). The transition results from the amplitude modulation of obliquity; no such transition occurs using constant amplitude forcing. **(c)** A spectrogram of the model response shows variability initially concentrated near $1/41$ ky^{-1} frequencies (dashed black line) and then toward lower $1/100$ ky^{-1} frequencies (other dashed black lines). Spectral energy is shaded according to the log of squared Fourier coefficients and normalized such that the largest values equal one. A spectrogram for a composite benthic-planktic marine δ^{18}O record (Huybers, 2007) is also shown for comparison **(d)**, along with the time series of δ^{18}O expressed as anomalies from the temporal mean **(e)**. Note that the y-axes for both δ^{18}O and ice volume are reversed.
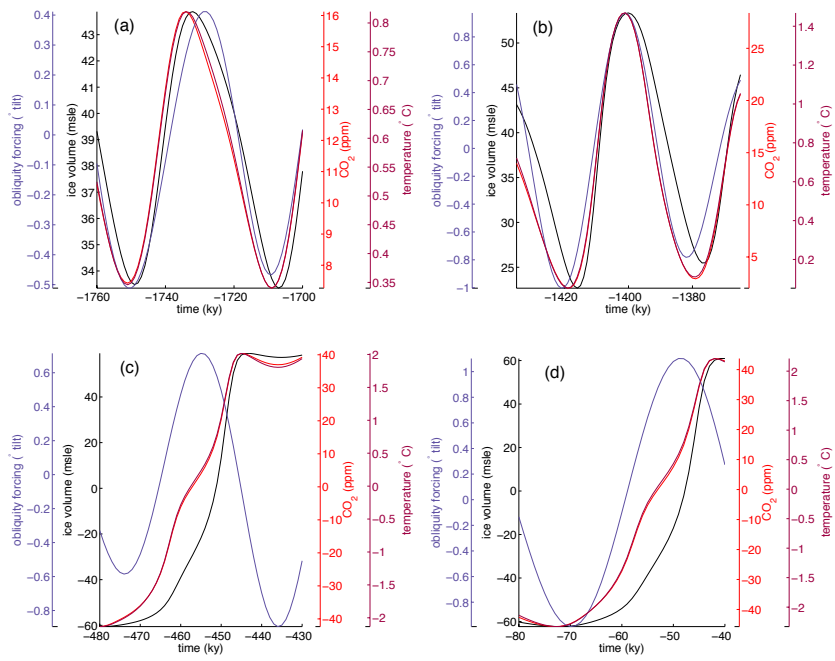
Figure 4: All model variables are shown for various deglacial sequences. There are unusual instances when obliquity lags behind ice volume **(a)**, though typically it leads **(b)** . During Late Pleistocene deglaciations changes in temperature lead changes in atmospheric CO_2 by several century **(c,d)**.
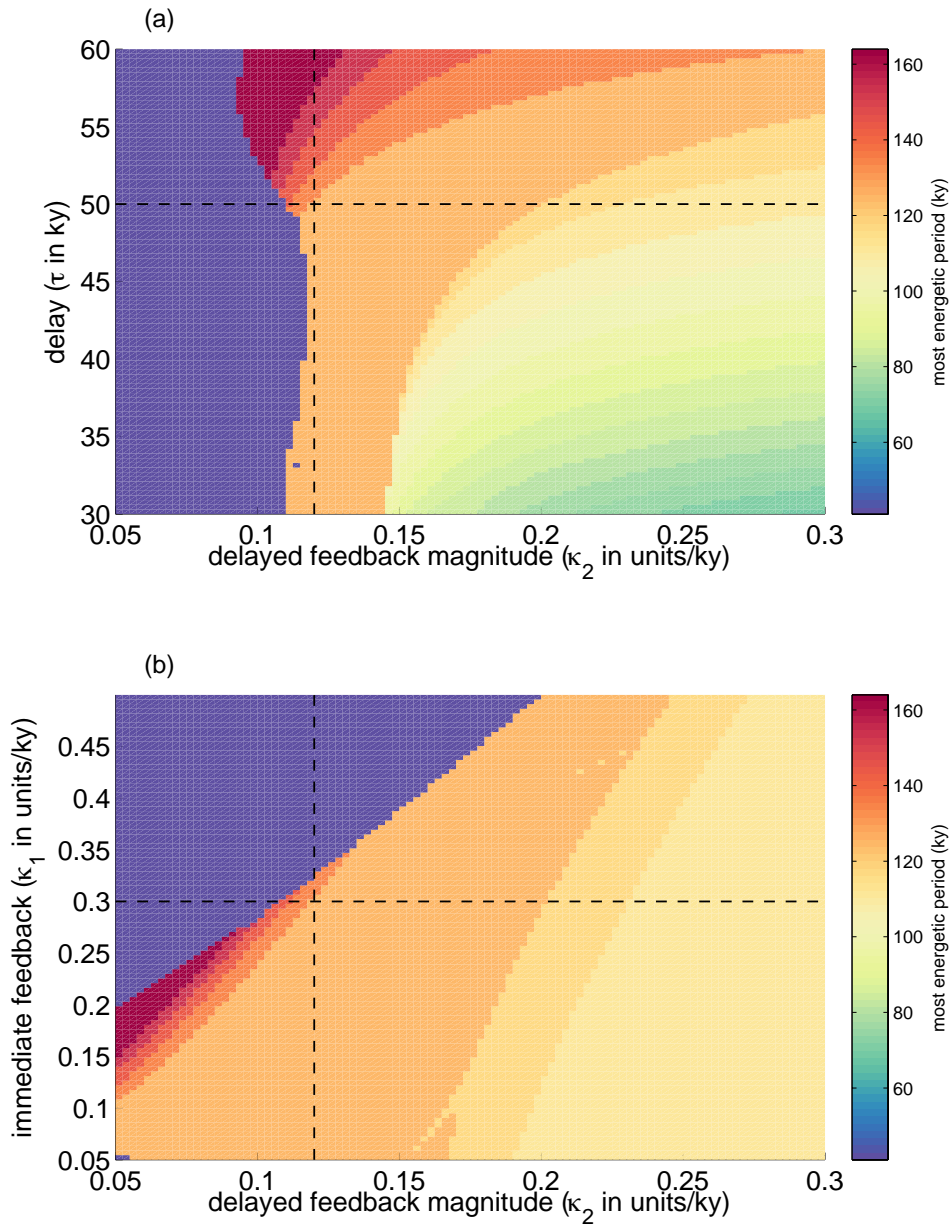
Figure 5: The dominant period of ice volume variability as a function of model parameters. **(a)** Period as a function of the magnitudes of κ_2 and δ. Greater magnitude feedback and smaller delay lead to shorter period glacial cycles. Note that the anomalous 41 ky period at $\kappa_2 = 0.11$ and $\delta = 33$ is an indication of dependence on initial conditions that arises near the boundaries between different period glacial cycles. Dashed black lines indicate default parameters. **(b)** is similar to (a) but for the dependence on κ_1 and κ_2.